In Situ Ellipsometric Monitoring of Gold Nanorod Metamaterials Growth

Published in:

Document Version:

Queen's University Belfast - Research Portal:
Link to publication record in Queen's University Belfast Research Portal

Research Article

In Situ Ellipsometric Monitoring of Gold Nanorod Metamaterials Growth

Frances Morgan,[†] Antony Murphy,[*,†] William Hendren,[†] Gregory Wurtz,[‡] and Robert J. Pollard[†]

[†]Centre for Nanostructured Media, The Queen's University of Belfast, Belfast BT7 1NN, United Kingdom
[‡]Department of Physics, University of North Florida, 1 UNF Drive, Jacksonville, Florida 32224, United States

S *Supporting Information*

ABSTRACT: An in situ transmission-based system has been designed to optically monitor the ellipsometry constants of a hyperbolic plasmonic metamaterial during electrochemical growth. The metamaterial, made from an array of vertically aligned gold nanorods, has demonstrated an unprecedented ability to manipulate the polarization of light using subwavelength thickness slabs, making in situ ellipsometric data a powerful tool in the controlled design of such components. In this work, we show practical proof-of-principle of this design method and rationalize the ellipsometric output on the basis of the modal properties of the nanorod metamaterial. The real-time optical monitoring setup provides excellent control and repeatability of nanostructure growth for the design of future ultrathin optical components. The performance of the ellipsometric method was also tested as a refractive index sensor. Monitoring refractive index changes near the metamaterial's epsilon near zero (ENZ) frequency showed a sensitivity on the order of 500°/RIU in the ellipsometric phase for a metamaterial that shows 250 nm/RIU sensitivity in its extinction.

KEYWORDS: in situ, nanostructures, plasmonics, ellipsometry, hyperbolic, metamaterial, nanorods
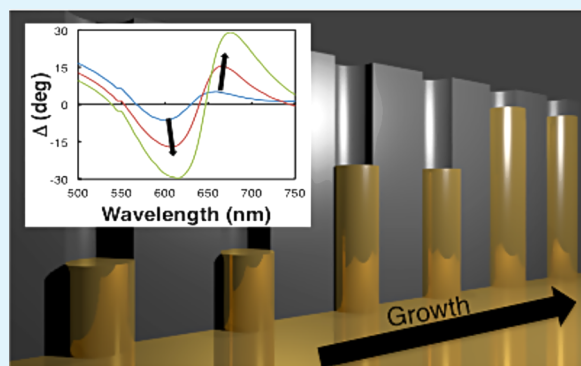
1. INTRODUCTION

Optical in situ monitoring during growth and etching processes is a common procedure in the semiconductor industry. It is seen as a noninvasive method for controlling the fabrication and morphology of precision thin films. The most frequently used techniques include reflectance anisotropy spectroscopy (RAS),[1,2] surface photon absorption (SPA),[3,4] and ellipsometry.[5,6] Although in situ optical monitoring of nanostructure fabrication is not unseen,[7−9] their characterization is largely performed post growth and is often done at the expense of destroying the sample. Real-time in situ optical monitoring could open the door to the scalable and repeatable production of functional nanostructured systems, in particular resonant plasmonic nanostructures, whose optical properties are strongly sensitive to geometrical parameters, including refractive index, size, and shape.[10,11] Real-time monitoring can also show the interplay and development of new modes as the growth of complex nanostructures progresses, providing a better understanding of their underlying behavior, but most of all allowing one to design optical functionalities on demand in vivo.

One of the most comprehensively studied plasmonic nanostructured systems, and also one of the most promising for practical implementation based on its ease and scalability to fabricate, are nanorod-based metamaterials.[12] Nanorods of various materials can be grown in solution chemically[13,14] or by electrodeposition into an alumina template.[15−18] Gold nanorods are particularly interesting as they exhibit anisotropic optical properties throughout the visible and near-infrared spectral range, a property related to localized surface plasmon resonances (LSPR) across their long and short axes.[19] When incorporated into an alumina template of suitable geometry, LSPR supported by nanorods when isolated, electromagnetically couple providing the formed metamaterial with unique optical properties that can be tailored to address a range of applications from biosensing[20] to ultrafast optical switching.[21]

It has recently been demonstrated that such a uniaxial nanorod metamaterial can be used as an ultrathin optical component to effectively manipulate the polarization of light.[22,23] In particular, it was shown that both the reflection from and transmission through a $\lambda/20$ thick slab of the metamaterial can provide a 90° linear polarization rotation, a performance not observed in natural materials. The polarization conversion efficiency comes from the plasmonic nature of the modes supported by the metamaterial, providing a significant difference between the ordinary and extraordinary permittivities. The ability to manipulate the polarization of light is essential in many applications including liquid crystal displays,[24,25] medical diagnostics,[26] and telecommunications.[22] For example, such hyperbolic metamaterials could replace conventional birefringent materials, such as rutile,[27] which require tens
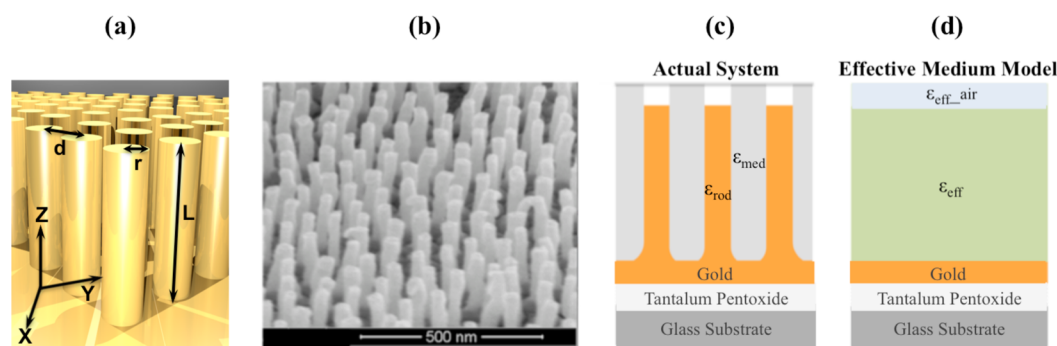
Figure 1. (a) 3D schematic of the nanorod system indicating geometric parameters including nanorod length L, radius r, and spacing d. (b) SEM of a gold nanorod assembly after AAO template removal. The viewing angle is 52°. (c) Schematic diagram of the full nanorod metamaterial system showing the different components, and (d) the associated geometry for the effective medium model used in the calculations.
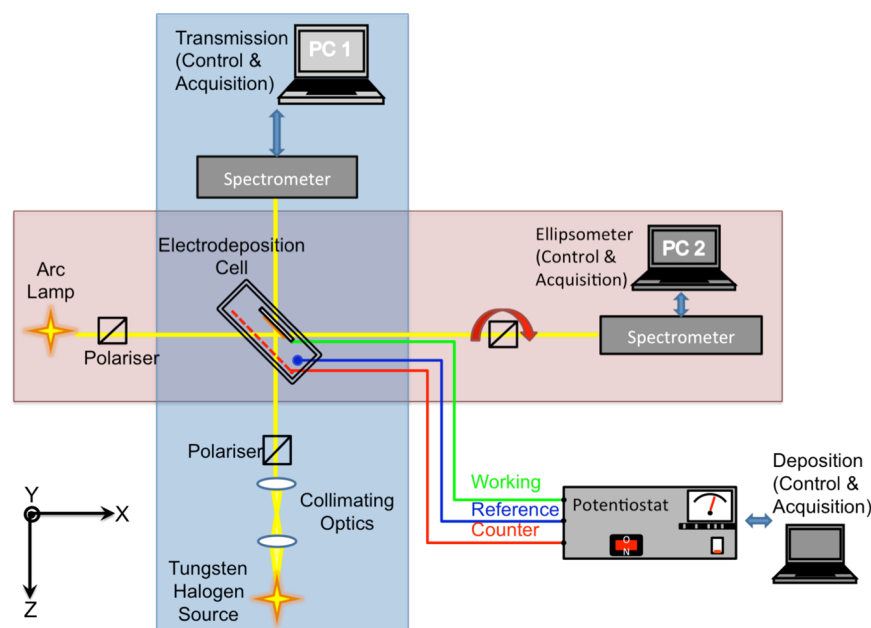
Figure 2. Schematic representation of the in situ optical setup used to monitor metamaterial growth. The transmission measurement setup is shown in blue; the ellipsometric measurement setup is shown in red. Also shown is the potentiostat controlling electrodepositon.

of micrometers to achieve similar polarization conversions. However, for nanorod metamaterial polarization converters to be adopted for practical use, precise engineering of the anisotropy in the metamaterial is required.

In this paper, we have devised a simple optical setup whereby the ellipsometric constants and the transmittance of the metamaterial are measured simultaneously during the electrochemical growth process. This in situ measurement technique not only improves upon the control and repeatability with which these metamaterials may be fabricated, but also provides a means for understanding their optical response as their modal structure evolves during growth. Additionally, given the importance of sensing in many applied fields, as in functional label-free biosensing, the sensitivity performance of the ellipsometric data to refractive index changes is further demonstrated.

2. METHODS

2.1. Nanorod Metamaterial Fabrication. The fabrication technique used to create gold (Au) nanorod metamaterials has been published elsewhere in great detail.[15] The general geometry of the system is presented in Figure 1. Briefly, thin films of tantalum

pentoxide (Ta_2O_5), gold, and aluminum are deposited using magnetron sputtering to form the sample template. The aluminum top layer is then anodized in a 0.3 M sulfuric acid bath at 35 V to produce an array of pores with an average center-to-center separation of $d = 80$ nm. In this instance the thickness of the aluminum layer was set to 400 nm. The aluminum is then chemically etched in a 30 mM NaOH solution to remove the barrier layer at the base of the pores. This step is also used to controllably widen the pores, thus determining the diameter, $2r$, of the nanorods electrochemically grown in the subsequent step. For the present study, the electrodeposition of gold was carried out at a constant voltage (-0.45 V) in a gold chloride electrolyte solution to grow nanorods of various lengths L in the pores. This final step completes the fabrication of the metamaterial (Figure 1b).

2.2. Metamaterial Structural Characterization. An experimental setup was designed to simultaneously measure the transmission and ellipsometric phase angles of the gold nanorods based metamaterial in situ during growth (Figure 2). The sample was mounted in the electrodeposition cell to probe both the sample's extinction and ellipsometric parameters in transmission at an incidence angle of 45°. This configuration is chosen for diagnostics purposes only, to allow probing transmission and ellipsometric parameters simultaneously for the same angle of incidence on different paths. More generally, both
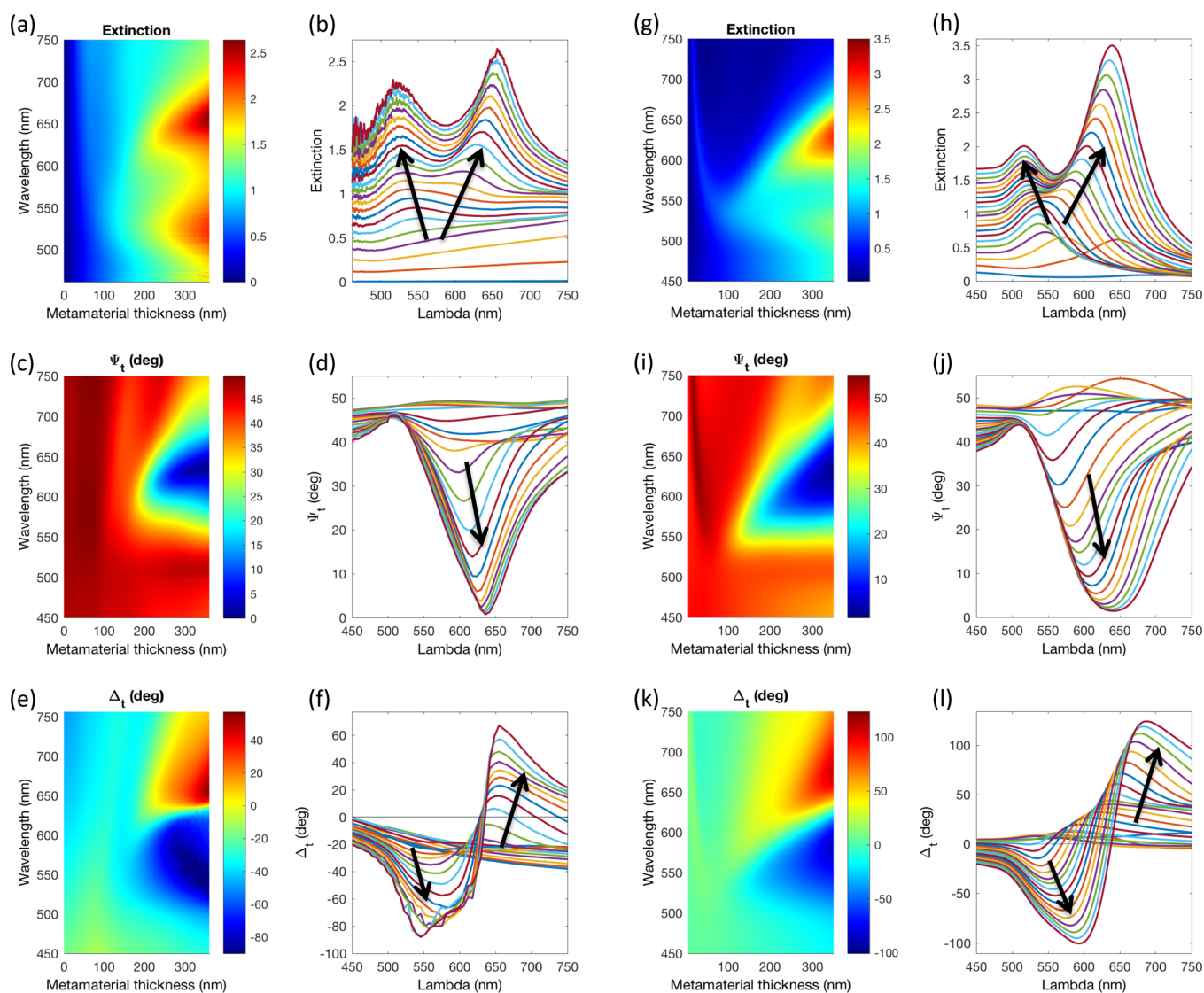
Figure 3. In situ optical and ellipsometric response of the nanorod metamaterial measured during metamaterial growth. Average nanorod diameter and inter-rod spacing as determined by the template are 38 and 70 nm, respectively. The matematerial growth is characterized by its thickness or equivalently the nanorod length. (a) Surface plot of the monitored extinction ($-\log_{10}$(Transmission)) spectra as a function of metamaterial thickness, assuming a linear relationship between growth time and metamaterial thickness, and (b) associated 2D cross-sectional plot. (g, h) Corresponding effective medium calculations. (c) Surface plot showing the spectral behavior of the ellipsometric amplitude angle (Ψ_t) as a function of metamaterial thickness during growth, and (d) associated 2D cross-sectional plot. (i, j) Corresponding effective medium calculations. (e) Surface plot showing the spectral behavior of the ellipsometric phase angle (Δ_t) as a function of metamaterial thickness during growth, and (f) associated 2D cross-sectional plot. (k, l) Corresponding effective medium calculations. The general trend of the plotted data with increasing metamaterial thickness is indicated by arrows in the respective cross sections.

measured quantities can be obtained from ellipsometric measurements alone, therefore lifting the constraint on angle of incidence.

The blue outline in Figure 2 highlights the transmission measurement arm of the setup. The incident light, produced by a Tungsten halogen source in the visible and near-infrared regime (400−900 nm), is incident to the sample through a series of optical components controlling collimation and polarization. The latter was set to p-polarized light, where the electric field oscillates with a component both along the length and the diameter of the nanorods, i.e. in the (x, z) plane of Figure 1a and Figure 2, thus simultaneously probing both ordinary (x) and extraordinary (z) axis of the metamaterial. Transmission measurements recorded the spectrum of the light source after transit through the sample via an optical fiber bundle coupled to a spectrometer. The transmission and corresponding extinction were plotted during electrodeposition, giving an indication of the height of the nanorods and in turn providing direct control over their growth. The electrodeposition voltage and

corresponding deposition current were also recorded across the working electrode and a platinum wire reference, giving additional information on the nanostructure growth characteristics.[15]

2.3. In Situ Spectroscopic Ellipsometry. The red outlined arm in Figure 2 shows a schematic of the in situ ellipsometry measurement setup. For this proof-of-principle experiment, it is placed orthogonal to the transmission arm in order to provide both arms with the same angle of incidence. The ellipsometric measurements provide ellipsometric angles which are a measure of both amplitude ratio and phase shift between the p- and s-components of the light transmitted by the nanorod metamaterial, where the p- and s-components of the incident electric field are those in the (x, z) plane and along the y-axis, respectively (see Figures 1 and 2). Here we chose characterizing the ellipsometric angles in transmission as they provide for a direct insight into the hyperbolic properties of the metamaterial as will be shown below. When taken in transmission, the ellipsometric angles Ψ and Δ are defined by the following equation

$$\tan \Psi e^{-i\Delta} = \frac{t_p}{t_s}$$

where t_p and t_s are the transmission coefficient for p- and s-polarized light, respectively, $\tan\Psi = |E_p|/|E_s|$, with $|E_p|$ and $|E_s|$ the norm of the transmitted electric field for p- and s-polarized light, and Δ is the relative phase difference between p-and s-polarized transmitted light. A commercial M-88 rotating analyzer ellipsometer (J. A. Woollam, Inc.) was used to perform the standard ellipsometry measurements. It was equipped with a Xenon arc lamp source for simultaneous measurements in the [450 nm-750 nm] wavelengths range; a full spectrum was completed in 1/20 s and the WVASE software was used to compute the corresponding ellipsometric components Ψ and Δ during nanorod growth. The instrument was mounted on an automated goniometer stage for measurements at variable angles of incidence, for postdeposition characterization.

2.4. Effective Medium Theory Modeling. The unique optical properties of gold nanorod metamaterials are ultimately governed by LSPRs.[19,28] Their optical response can be modeled using effective medium theories (EMTs), simplifying composite layers of nanoscale metallic inclusions with position and frequency-dependent permittivity $\varepsilon_{Au}(\vec{r},\omega)$ embedded in a matrix material with position and frequency-dependent permittivity $\varepsilon_d(\vec{r},\omega)$, into a layer with a frequency-dependent effective permittivity $\varepsilon_{eff}(\omega)$ (Figure 1c, d).[19,29−31] This effective permittivity can be found from the metamaterial's components volume fractions and polarizabilities within a Maxwell-Garnett approximation as shown before by R. Atkinson et al.[19] In this formulation, the metamaterial layer is then considered a uniaxial anisotropic film (Figure 1d) with an effective permittivity expressed in the Cartesian referential system of Figure 1 as $\varepsilon_{eff}(\omega) =$ diag $(\varepsilon_x(\omega)$, $\varepsilon_y(\omega) = \varepsilon_x(\omega)$, $\varepsilon_z(\omega))$, where z, taken along the nanorod length, corresponds to the extraordinary axis of the metamaterial, while the ordinary axis lies in the (x, y) plane. Gold nanorod-based metamaterials are attracting a lot of attention due to their anisotropic optical response in the vicinity and beyond the so-called epsilon-near-zero (ENZ) frequency which marks the transition between elliptic and hyperbolic dispersion regimes.[22,32,33] Hyperbolic materials are interesting in many aspects, as they show strong enhancement of spontaneous emission,[34] negative refraction[35,36] and enhanced super-lensing effects.[37,38] A material is said to show hyperbolic dispersion when the electric permittivity or magnetic permeability effective tensors has components of different signs. The nanorod metamaterial considered here typically offers two dispersion regimes. An elliptic dispersion regime where both $\varepsilon_{x,y} > 0$ and $\varepsilon_z > 0$, and a hyperbolic dispersion, where $\varepsilon_{x,y} > 0$ and $\varepsilon_z < 0$, with the transition between the two regimes being characterized by the ENZ frequency for which $|\varepsilon_z| \to 0$.[39] Although the hyperbolic dispersion offers important optical properties,[20,40] operating in the vicinity of the ENZ regime $|\varepsilon_z| \approx 0$ also provides highly desirable linear and nonlinear optical properties as additional waves can be excited in low-loss metamaterials, i.e., when Im $(\varepsilon_z) \to 0$. This has been shown to provide enhanced nonlinear optical properties, for example,[21,41] but has also been the basis for spectral refractive index characterization.[42] These effects all rely on the resonant response of the metamaterial as it transitions from the elliptic and hyperbolic dispersion regimes. One particularly appealing property of the nanorod metamaterial is the extensive flexibility it provides in tuning the ENZ frequency by geometrical means. For example, by using nanorods made of Au the ENZ frequency was shown to be continuously tunable in the 520−1700 nm range by controlling selected geometrical properties, such as the nanorod length, diameter, spacing, or the refractive index of the embedding medium.[43]

3. RESULTS AND DISCUSSION

The in situ apparatus was used to characterize the optical properties of a gold nanorod metamaterial during growth. The nanorods were grown to a final height of approximately 350 nm in 180 s, giving an average growth rate of ~2 nm/s, and have average dimensional parameters of 38 nm in diameter and 80 nm in center-to-center spacing, as set by the AAO template.

Figure 3a, b shows the extinction $-\log_{10}$(Transmission) of the metamaterial as measured as a function of wavelength and metamaterial thickness, along with the corresponding ellipsometric parameters Ψ (Figure 3c, d) and Δ (Figure 3e, f) obtained simultaneously during growth. The corresponding EMT calculation results are shown in Figure 3g−l providing excellent agreement with the experimental observations, although it must be noted that the assumed metamaterial geometry during growth, including the average growth rate, can be at the origin of small discrepancies between experimental and EMT observations in Figure 3. In particular, the growth dynamics is a complex phenomenon and its assumed linear time behavior, especially at early stages, is an approximation that affects the comparison between experiments and calculations. Here we are making use of the EMT results to provide a general understanding of the experimental data and rationalize the ellipsometric response to allow their use in the design of ultrathin phase-shaping metamaterials with chosen and controlled polarization properties. As a result, approximations on electrochemical growth dynamics and metamaterial geometry during the growth do not affect the generality of our analysis below.

The overall extinction of the metamaterial increases steadily during growth as Au is deposited into the alumina pores to form the rods (Figure 3a, b). After about 100 s of growth time, or for a metamaterial thickness of about 200 nm, two distinct resonances can be observed, one at a wavelength of around 550 nm and another at around 625 nm. The short-wavelength peak, referred to as the T-mode in the literature, is associated with a transverse LSPR originating from free electrons oscillating across the diameter of the nanorods.[19,42] The second peak, observed in the extinction at around 625 nm, corresponds to the resonant excitation of the free electron density along the long axis of the rods and is referred to as the L-mode in the literature.[19,42] The field distribution for these two modes is presented in Figure S1. In contrast to the T-mode, the L-mode is delocalized over several nanorods and arises from Re $(\varepsilon_z) \to 0$, signaling the transition of the nanorod metamaterial from an elliptic to a hyperbolic dispersion.[40,44] Further metamaterial growth leads to the observation of an increased spectral splitting of the two modes with a blue-shift of the T-mode to a wavelength of about 525 nm and a red-shift of the L-mode to about 650 nm. The spectral behavior of these resonances and their underlying nature as a function of metamaterial thickness has been thoroughly discussed elsewhere.[19,39,42,43,45,46] The analysis of Ψ in Figure 3c, d is consistent with the measured extinction of Figure 3a, b. Indeed, for $|E_p| > |E_s|$, we expect $\tan\Psi > 1$ i.e., $45° < \Psi \leq 90°$, whereas for $|E_p| < |E_s|$ we expect $\tan\Psi < 1$, i.e., $0 \leq \Psi < 45°$ with the case $|E_p| = |E_s|$ corresponding to $\tan\Psi = 1$ and $\Psi = 45°$. Figure 3c, d shows that the T-mode maximum corresponds to $\Psi \approx 45°$, which is expected for an angle of incidence of 45°, whereas $\Psi \to 0°$ at the L-mode maximum with most of the transmitted field transmitted by the metamaterial in this spectral range being s-polarized. Again, this general behavior is also retrieved from the EMT calculations of Figure 3i−j. In fact plotting Ψ in Figure 4a such as $\tan\Psi = |E_p|/|E_s| \approx \sqrt{T_p/T_s}$ where T_p and T_s are the metamaterial's transmittance for p- and s-polarization, respectively, reproduces both the measured (Figure 3c) and EMT (Figures 3i and 4c) results both qualitatively and quantitatively very well, providing a direct link between Ψ and the resonant response of the metamaterial.
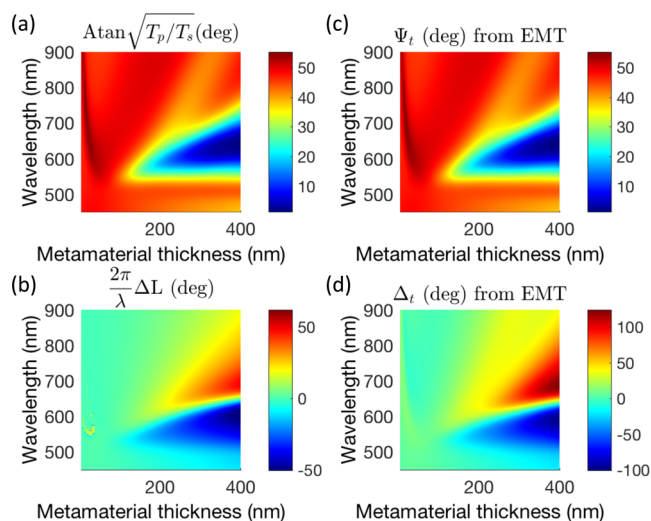
Figure 4. (a) Amplitude angle Ψ calculated assuming $\tan \Psi \sim \sqrt{T_p/T_s}$ and (b) Phase angle Δ calculated assuming $\Delta \approx \Delta\varphi = \frac{2\pi}{\lambda_0}(n_p L_p - n_s L_s)$. (c, d) Corresponding EMT calculated Ψ and Δ respectively.

Although the Ψ signal shows an absorptive shape, the phase signal Δ of Figure 3e, f shows a differential shape for metamaterial thicknesses exceeding ∼150 nm. This thickness corresponds to the transition from the assembly of nanorods acting as an ensemble of weakly interacting resonators to a metamaterial made of strongly interacting nanorods. In fact, the differential shape is a signature of the dispersive behavior of the metamaterial transitioning between the elliptic and hyperbolic dispersion regimes. In the elliptic regime, the s-polarized field lags the p-polarized field (blue region in Figure 3e), while the opposite situation arises in the hyperbolic regime (red region in Figure 3e). Again, this observation is confirmed through the EMT calculations of Figure 3e, f and Figure 4c, d. Further insight can be provided simply by expressing the phase difference $\Delta\varphi$ experienced by p- and s-polarized fields as they transmit through the metamaterial as $\Delta\varphi = \frac{2\pi}{\lambda_0}(n_p L_p - n_s L_s)$, where λ_0 is the free-space wavelength of the transmitted light, n_p and n_s are the respective refractive indices experienced by p- and s-polarized fields, and L_p and L_s are the geometrical pathlengths for p- and s-polarized fields, respectively. Expressions for the refractive index are chiefly those governing the propagation of light in uniaxial materials such as $n_p = \sqrt{\varepsilon_p} = \sqrt{\varepsilon_x + \sin^2\theta\left(1 - \frac{\varepsilon_x}{\varepsilon_z}\right)}$, where θ is the angle of incidence in air as measured from the z-axis. To a first approximation the pathlengths can be expressed as $L_{p,s} = \frac{d}{\cos\theta_{p,s}}$, where the angle of refraction for p- and s-polarized fields $\theta_{p,s}$ is found using Snell's law of refraction $\sqrt{\varepsilon_{sub}} \sin\theta = \mathrm{Re}(\sqrt{\varepsilon_{p,x}}) \sin\theta_{p,s}$. The resulting map of $\Delta\varphi$, plotted in Figure 4b, reproduces the main features of the experimental observations of Figure 3e and is in excellent qualitative agreement with the EMT calculations of Figure 3k and Figure 4d. The change in sign of the dephasing between p and s waves follows that of the term $(n_p L_p - n_s L_s)$. In fact, for incident angles exceeding normal incidence Snell's law predicts opposite trends for $n_p - n_s$ and $L_p - L_s$, with the geometric

path length decreasing for increasing refractive index. As a result, $n_p - n_s$ and $L_p - L_s$ have a compensating effect on Δ but for the geometry considered here, the EMT calculations show that the behavior of Δ follows that of $n_p - n_s$ with max $(|n_p - n_s|) > 1$, whereas max $(|L_p - L_s|) \sim 50$ nm (see Figures S2−S4). For smaller metamaterial thicknesses, the length of the nanorods is close to their diameter leading to $n_p \approx n_s$, and subsequently $L_p \approx L_s$ and $\Delta \approx 0$ as measured in Figure 3c, d. As the length of the nanorods increases, the spectral behavior of Δ reflects that of $n_p - n_s$ with the s-polarized field leading the p-polarized field by more than 90° in the spectral range of elliptic dispersion to the s-polarized field lagging the p-polarized field by almost 60° in the spectral range of hyperbolic dispersion. The cross over where $\Delta = 0$ occurs at the L-mode resonance, slightly red-shifted from the ENZ frequency.

We finish our study by assessing the performance of the ellipsometric response of the nanorod metamaterial as a sensing platform. This is done in situ by monitoring the ellipsometric parameters in transmission while etching the alumina matrix surrounding the gold nanorod in the metamaterial. The change in the local refractive index resulting from this etch is a simple way of testing the refractive index sensitivity of ellipsometric measurements.[42] These will be evaluated against the more commonly used resonant changes resulting from the same refractive index change measured simultaneously via the extinction of the metamaterial.[42] For the experiment, the metamaterial is placed in a cell and immersed in 0.03 M sodium hydroxide solution with both ellipsometric parameters and extinction measured simultaneously as the alumina is gradually replaced by the etching solution changing the refractive index of the medium embedding the nanorods from $n \approx 1.6$ (alumina) to $n \approx 1.33$ (etching solution). With alumina as the embedding medium ($n \approx 1.6$), the metamaterial transitions from the elliptic to the hyperbolic regime at a wavelength of around 650 nm. This spectral range is the most sensitive to changes in refractive index when monitored in transmission as it corresponds to a resonance for incident TM-polarized light.[42] The ellipsometric spectra recorded for changing refractive index for both Ψ and Δ are shown in Figure 5. The spectral map for Ψ (Figure 5a) and Δ (Figure 5b) show the total shift in the transition wavelength of 70 nm from about 650 nm to about 580 nm. This corresponds to the full removal of the alumina template and replacement by the etching solution as the embedding refractive index is lowered from $n \approx 1.6$ to $n \approx 1.33$. This is confirmed by the extinction measurements (not shown) and gives a bulk sensitivity of approximately 250 nm/RIU when monitoring the L-mode resonance. This refractive index sensitivity is typical for nanorod-based metamaterials when monitored in transmission, although improvements by an order of magnitude can be achieved via both thermal annealing and by shifting the transition wavelength to lower frequencies, the latter increasing both sensitivity and dynamic range.[47]

Both Ψ and Δ data in Figure 5a, b demonstrate a behavior similar to our observations in Figure 3. The etching process starts at a time of around 30s (Figure 5a, b), following a nonlinear behavior until completion. This nonlinear behavior reflects both the density profile of the alumina matrix and is indicative of the etching mechanism.[42] In fact, the alumina matrix density increases gradually away from the pores containing the nanorods, corresponding also to a gradual increase in its refractive index. As a result, when subjected to the etching solution, the alumina is uniformly removed in the matrix along the length of the nanorods first, where the matrix
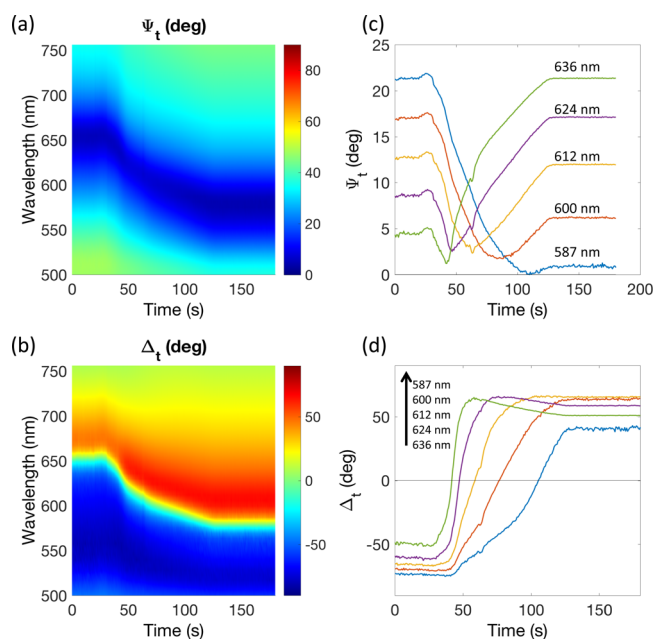
Figure 5. In situ time-dependent spectral map of (a) Ψ_t and (b) Δ_t monitoring changes in the refractive index of the matrix embedding the gold nanorods in the metamaterial as obtained through chemical etching. (c, d) Cross-section plots of a and b, respectively, showing the response of Ψ_t and Δ_t as monitored at selected wavelengths.

has the lowest density, creating a shell around the nanorods whose thickness grows outward toward neighboring nanorods as the etching process proceeds.[42,48] A saturation in the resonance shift is reached after a time of around 120s as a result of the spectral dispersion of the metamaterial in this spectral range, which makes the 250 nm/RIU sensitivity obtained from the extinction measurements a lower estimate value. Figure 5c, d shows selected cross-sections of Ψ and Δ, respectively, for various wavelengths in the 70 nm bandwidth of the resonance shift. Although the change in the amplitude parameter Ψ is limited to about 20° by the change in $\sqrt{T_p/T_s}$, as explained earlier the dephasing angle Δ varies by more than 150° during etching over the same spectral range as a result of the transition between elliptic and hyperbolic dispersions. This translates into a sensing sensitivity for Δ on the order of 500°/RIU, far exceeding the 250 nm/RIU sensitivity simultaneously obtained from the extinction of the same metamaterial. Importantly, it must be noted that unlike extinction, the amplitude in the variations of Δ, and Ψ to a lesser extent, are robust and relatively independent of bandwidth as long as some shift in the resonance occurs as a result of the refractive index change to trigger the transition between the elliptic and hyperbolic dispersion regimes. By replacing the sample cell with a flow-cell one could create a fully functional label-free biosensor, which benefits from dual optical outputs (phase and extinction) and an extremely sharp phase transition.

CONCLUSION

We studied the in situ ellipsometric response of a nanorod-based plasmonic metamaterial during growth. The ellipsometric angle data, measured in transmission, were rationalized with respect of the optical properties of the metamaterial on the basis of the extinction measurements, measured simultaneously. The ellipsometric angles show significant variations in the

vicinity of the ENZ frequency, where the metamaterial transitions from the elliptic to the hyperbolic dispersion regimes. In particular, the amplitude ratio shows an absorptive behavior with a maximum absolute change on the order of 50°, whereas the relative phase shows a dispersive behavior about the ENZ frequency with an amplitude change exceeding 150°. These variations have been associated with both the relative amplitude and relative phase of p- and s-waves transmitted through the metamaterial. The in situ ellipsometric data provide for a reliable method to grow these subwavelength-thick metamaterials to provide adjustable optical properties for applications as ultrathin polarization convertors. Additionally, we assessed the sensitivity of the ellipsometric parameters to changes in the refractive index within the metamaterial. Here changes in the relative phase exceed 500°/RIU for a metamaterial that shows a 250 nm/RIU sensitivity in its extinction.

ASSOCIATED CONTENT

Supporting Information

The Supporting Information is available free of charge on the ACS Publications website at DOI: 10.1021/acsami.7b04129.

Figures S1–S4 (PDF)

AUTHOR INFORMATION

Corresponding Author

*E-mail: antony.murphy@qub.ac.uk.

ORCID

Antony Murphy: 0000-0003-4039-9063

Author Contributions

The manuscript was written through contributions of all authors. All authors have given approval to the final version of the manuscript.

Notes

The authors declare no competing financial interest.

REFERENCES

(1) Döscher, H.; Hannappel, T. In Situ Reflection Anisotropy Spectroscopy Analysis of Heteroepitaxial Gap Films Grown on Si(100). *J. Appl. Phys.* **2010**, *107*, 123523.

(2) Reinhardt, F.; Richter, W.; Müller, A. B.; Gutsche, D.; Kurpas, P.; Ploska, K.; Rose, K. C.; Zorn, M. GaAs Surface Control During Metalorganic Vapor Phase Epitaxy by Reflectance Anisotropy Spectroscopy. *J. Vac. Sci. Technol., B: Microelectron. Process. Phenom.* **1993**, *11*, 1427−1430.

(3) Kobayashi, N. In-Situ Monitoring and Control of Surface Processes in Metalorganic Vapor Phase Epitaxy by Surface Photo-Absorption. *J. Cryst. Growth* **1994**, *145*, 1−11.

(4) Butler, J. E.; Bottka, N.; Sillmon, R. S.; Gaskill, D. K. In Situ, Real-Time Diagnostics of Omvpe Using Ir-Diode Laser Spectroscopy. *J. Cryst. Growth* **1986**, *77*, 163−171.

(5) Drévillon, B. Phase Modulated Ellipsometry from the Ultraviolet to the Infrared: In Situ Application to the Growth of Semiconductors. *Prog. Cryst. Growth Charact. Mater.* **1993**, *27*, 1−87.

(6) Johs, B.; Herzinger, C.; Dinan, J. H.; Cornfeld, A.; Benson, J. D.; Doctor, D.; Olson, G.; Ferguson, I.; Pelczynski, M.; Chow, P.; Kuo, C. H.; Johnson, S. Real-Time Monitoring and Control of Epitaxial Semiconductor Growth in a Production Environment by in Situ Spectroscopic Ellipsometry. *Thin Solid Films* **1998**, *313–314*, 490–495.

(7) He, Y.; Cheng, Y.; Zhao, J.; Li, X.-Z.; Gong, Q.; Lu, G. Light Driving and Monitoring Growth of Single Gold Nanorods. *J. Phys. Chem. C* **2016**, *120*, 16954–16959.

(8) Reinhold-Lopez, K.; Braeuer, A.; Romann, B.; Popovska-Leipertz, N.; Leipertz, A. Simultaneous in Situ Raman Monitoring of the Solid and Gas Phases During the Formation and Growth of Carbon Nanostructures inside a Cold Wall Ccvd Reactor. *Carbon* **2014**, *78*, 164–180.

(9) Strelcov, E.; Davydov, A. V.; Lanke, U.; Watts, C.; Kolmakov, A. In Situ Monitoring of the Growth, Intermediate Phase Transformations and Templating of Single Crystal Vo2 Nanowires and Nanoplatelets. *ACS Nano* **2011**, *5*, 3373–3384.

(10) Kelly, K. L.; Coronado, E.; Zhao, L. L.; Schatz, G. C. The Optical Properties of Metal Nanoparticles: The Influence of Size, Shape, and Dielectric Environment. *J. Phys. Chem. B* **2003**, *107*, 668.

(11) Barnes, W. L.; Dereux, A.; Ebbesen, T. W. Surface Plasmon Subwavelength Optics. *Nature* **2003**, *424*, 824–830.

(12) Perezjuste, J.; Pastorizasantos, I.; Lizmarzan, L.; Mulvaney, P. Gold Nanorods: Synthesis, Characterization and Applications. *Coord. Chem. Rev.* **2005**, *249*, 1870–1901.

(13) Jana, N. R.; Gearheart, L.; Murphy, C. J. Wet Chemical Synthesis of High Aspect Ratio Cylindrical Gold Nanorods. *J. Phys. Chem. B* **2001**, *105*, 4065.

(14) Nikoobakht, B.; El-Sayed, M. A. Preparation and Growth Mechanism of Gold Nanorods (Nrs) Using Seed-Mediated Growth Method. *Chem. Mater.* **2003**, *15*, 1957–1962.

(15) Evans, P.; Hendren, W. R.; Atkinson, R.; Wurtz, G. A.; Dickson, W.; Zayats, A. V.; Pollard, R. J. Growth and Properties of Gold and Nickel Nanorods in Thin Film Alumina. *Nanotechnology* **2006**, *17*, 5746–5753.

(16) Meng, G.; Cao, A.; Cheng, J.-Y.; Vijayaraghavan, A.; Jung, Y. J.; Shima, M.; Ajayan, P. M. Ordered Ni Nanowire Tip Arrays Sticking out of the Anodic Aluminum Oxide Template. *J. Appl. Phys.* **2005**, *97*, 064303.

(17) Zong, R. L.; Zhou, J.; Li, B.; Fu, M.; Shi, S. K.; Li, L. T. Optical Properties of Transparent Copper Nanorod and Nanowire Arrays Embedded in Anodic Alumina Oxide. *J. Chem. Phys.* **2005**, *123*, 094710.

(18) Evans, P. R.; Kullock, R.; Hendren, W. R.; Atkinson, R.; Pollard, R. J.; Eng, L. M. Optical Transmission Properties and Electric Field Distribution of Interacting 2d Silver Nanorod Arrays. *Adv. Funct. Mater.* **2008**, *18*, 1075–1079.

(19) Atkinson, R.; Hendren, W.; Wurtz, G.; Dickson, W.; Zayats, A.; Evans, P.; Pollard, R. Anisotropic Optical Properties of Arrays of Gold Nanorods Embedded in Alumina. *Phys. Rev. B: Condens. Matter Mater. Phys.* **2006**, *73*, 235402.

(20) Kabashin, A. V.; Evans, P.; Pastkovsky, S.; Hendren, W.; Wurtz, G.; Atkinson, R.; Pollard, R.; Podolskiy, V.; Zayats, A. Plasmonic Nanorod Metamaterials for Biosensing. *Nat. Mater.* **2009**, *8*, 867–871.

(21) Wurtz, G. A.; Pollard, R.; Hendren, W.; Wiederrecht, G.; Gosztola, D.; Podolskiy, V. A.; Zayats, A. V. Designed Ultrafast Optical Nonlinearity in a Plasmonic Nanorod Metamaterial Enhanced by Nonlocality. *Nat. Nanotechnol.* **2011**, *6*, 107.

(22) Ginzburg, P.; Fortuño, F. J. R.; Wurtz, G. A.; Dickson, W.; Murphy, A.; Morgan, F.; Pollard, R. J.; Iorsh, I.; Atrashchenko, A.; Belov, P. A.; Kivshar, Y. S.; Nevet, A.; Ankonina, G.; Orenstein, M.; Zayats, A. V. Manipulating Polarization of Light with Ultrathin Epsilon-near-Zero Metamaterials. *Opt. Express* **2013**, *21*, 14907.

(23) Kullock, R.; Hendren, W. R.; Hille, A.; Grafström, S.; Evans, P. R.; Pollard, R. J.; Atkinson, R.; Eng, L. M. Polarization Conversion through Collective Surface Plasmons in Metallic Nanorod Arrays. *Opt. Express* **2008**, *16*, 21671–21681.

(24) Stalder, M.; Schadt, M. Linearly Polarized Light with Axial Symmetry Generated by Liquid-Crystal Polarization Converters. *Opt. Lett.* **1996**, *21*, 1948–1950.

(25) Yang, X.; Yan, Y.; Jin, G. Polarized Light-Guide Plate for Liquid Crystal Display. *Opt. Express* **2005**, *13*, 8349–8356.

(26) Hunter, D. G.; Patel, S. N.; Guyton, D. L. Automated Detection of Foveal Fixation by Use of Retinal Birefringence Scanning. *Appl. Opt.* **1999**, *38*, 1273–1279.

(27) Cardona, M.; Harbeke, G. Optical Properties and Band Structure of Wurtzite-Type Crystals and Rutile. *Phys. Rev.* **1965**, *137*, A1467–A1476.

(28) Huang, H. J.; Yu, C.; Chang, H. C.; Chiu, K. P.; Ming Chen, H.; Liu, R. S.; Tsai, D. P. Plasmonic Optical Properties of a Single Gold Nano-Rod. *Opt. Express* **2007**, *15*, 7132–7139.

(29) Gao, D. L.; Gao, L.; Qiu, C. W. Birefringence-Induced Polarization-Independent and Nearly All-Angle Transparency through a Metallic Film. *Europhys. Lett.* **2011**, *95*, 34004.

(30) Elser, J.; Wangberg, R.; Podolskiy, V. A.; Narimanov, E. E. Nanowire Metamaterials with Extreme Optical Anisotropy. *Appl. Phys. Lett.* **2006**, *89*, 261102.

(31) Wood, B.; Pendry, J.; Tsai, D. Directed Subwavelength Imaging Using a Layered Metal-Dielectric System. *Phys. Rev. B: Condens. Matter Mater. Phys.* **2006**, *74*, 115116.

(32) Schilling, J. Uniaxial Metallo-Dielectric Metamaterials with Scalar Positive Permeability. *Phys. Rev. E* **2006**, *74*, 046618.

(33) Poddubny, A.; iorsh, I.; Belov, P.; Kivshar, Y. Hyperbolic Metamaterials. *Nat. Photonics* **2013**, *7*, 948–967.

(34) Jacob, Z.; Smolyaninov, I. I.; Narimanov, E. E. Broadband Purcell Effect: Radiative Decay Engineering with Metamaterials. *Appl. Phys. Lett.* **2012**, *100*, 181105.

(35) Belov, P. Backward Waves and Negative Refraction in Uniaxial Dielectrics with Negative Dielectric Permittivity Along the Anisotropy Axis. *Microwave and Optical Technology Letters* **2003**, *37*, 259–263.

(36) Lindell, I. V.; Tretyakov, S. A.; Nikoskinen, K. I.; Ilvonen, S. Bw Media—Media with Negative Parameters, Capable of Supporting Backward Waves. *Microwave and Optical Technology Letters* **2001**, *31*, 129–133.

(37) Liu, Z.; Lee, H.; Xiong, Y.; Sun, C.; Zhang, X. Far-Field Optical Hyperlens Magnifying Sub-Diffraction-Limited Objects. *Science* **2007**, *315*, 1686.

(38) Rho, J.; Ye, Z.; Xiong, Y.; Yin, X.; Liu, Z.; Choi, H.; Bartal, G.; Zhang, X. Spherical Hyperlens for Two-Dimensional Sub-Diffractional Imaging at Visible Frequencies. *Nat. Commun.* **2010**, *1*, 143.

(39) Pollard, R.; Murphy, A.; Hendren, W.; Evans, P.; Atkinson, R.; Wurtz, G.; Zayats, A.; Podolskiy, V. Optical Nonlocalities and Additional Waves in Epsilon-near-Zero Metamaterials. *Phys. Rev. Lett.* **2009**, *102*, 127405.

(40) Vasilantonakis, N.; Nasir, M. E.; Dickson, W.; Wurtz, G. A.; Zayats, A. V. Bulk Plasmon-Polaritons in Hyperbolic Nanorod Metamaterial Waveguides. *Laser Photonics Rev.* **2015**, *9*, 345–353.

(41) Neira, A. D.; Wurtz, G. A.; Ginzburg, P.; Zayats, A. V. Ultrafast All-Optical Modulation with Hyperbolic Metamaterial Integrated in Si Photonic Circuitry. *Opt. Express* **2014**, *22*, 10987–10994.

(42) Evans, P. R.; Wurtz, G. A.; Atkinson, R.; Hendren, W.; O'Connor, D.; Dickson, W.; Pollard, R. J.; Zayats, A. V. Plasmonic Core/Shell Nanorod Arrays: Subattoliter Controlled Geometry and Tunable Optical Properties. *J. Phys. Chem. C* **2007**, *111*, 12522.

(43) Nasir, M. E.; Peruch, S.; Vasilantonakis, N.; Wardley, W. P.; Dickson, W.; Wurtz, G. A.; Zayats, A. V. Tuning the Effective Plasma Frequency of Nanorod Metamaterials from Visible to Telecom Wavelengths. *Appl. Phys. Lett.* **2015**, *107*, 121110.

(44) Wurtz, G. A.; Dickson, W.; O'Connor, D.; Atkinson, R.; Hendren, W.; Evans, P.; Pollard, R.; Zayats, A. V. Guided Plasmonic Modes in Nanorod Assemblies: Strong Electromagnetic Coupling Regime. *Opt. Express* **2008**, *16*, 7460–7470.

(45) Wurtz, G. A.; Zayats, A. V. Nonlinear Surface Plasmon Polaritonic Crystals. *Laser Photonics Rev.* **2008**, *2*, 125–135.

(46) Tsai, K. T.; Wurtz, G. A.; Chu, J. Y.; Cheng, T. Y.; Wang, H. H.; Krasavin, A. V.; He, J. H.; Wells, B. M.; Podolskiy, V. A.; Wang, J. K.;

Wang, Y. L.; Zayats, A. V. Looking into Meta-Atoms of Plasmonic Nanowire Metamaterial. *Nano Lett.* **2014**, *14*, 4971−4976.

(47) Vasilantonakis, N.; Wurtz, G. A.; Podolskiy, V. A.; Zayats, A. V. Refractive Index Sensing with Hyperbolic Metamaterials: Strategies for Biosensing and Nonlinearity Enhancement. *Opt. Express* **2015**, *23*, 14329−14343.

(48) Wurtz, G. A.; Evans, P. R.; Hendren, W.; Atkinson, R.; Dickson, W.; Pollard, R. J.; Harrison, W.; Bower, C.; Zayats, A. V. Molecular Plasmonics with Tunable Exciton-Plasmon Coupling Strength in J-Aggregate Hybridized Au Nanorod Assemblies. *Nano Lett.* **2007**, *7*, 1297−1303.